Wear-resistant magnetic thin film material based on a $Ti_{1-x}Fe_xC_{1-y}$ nanocomposite alloy

Stojanka Bijelovic,[1] Mikael Råsander,[2] Ola Wilhelmsson,[3] Erik Lewin,[3] Biplab Sanyal,[2] Ulf Jansson,[3] Olle Eriksson,[2] and Peter Svedlindh[1]

[1]*Department of Engineering Science, Uppsala University, P.O. Box 534, SE-751 21 Uppsala, Sweden*

[2]*Department of Physics and Materials Science, Uppsala University, P.O. Box 530, SE-751 21 Uppsala, Sweden*

[3]*Department of Materials Chemistry, Uppsala University, P.O. Box 538, SE-751 21 Uppsala, Sweden*

(Received 29 June 2009; revised manuscript received 3 December 2009; published 7 January 2010)

In this study we report on the film growth and characterization of thin (approximately 50-nm-thick) Ti-Fe-C films deposited on amorphous quartz. The experimental studies have been complemented by first-principles density-functional theory (DFT) calculations. Upon annealing of as-prepared films, the composition of the metastable Ti-Fe-C film changes. With increasing annealing time, there is a depletion of iron close to the surface of the film, while regions enriched in iron are simultaneously formed deeper into the film. Both the magnetic ordering temperature and the saturation magnetization changes significantly upon annealing. The DFT calculations show that the critical temperature and the magnetic moment both increase with increasing Fe and C-vacancy concentration. The formation of the metastable iron-rich Ti-Fe-C compound is reflected in the strong increase in the magnetic ordering temperature. Eventually, after enough annealing time ($\geq$10 min), nanocrystalline α-Fe starts to precipitate, the amount and size of which can be controlled by the annealing procedure; after 20 min of annealing, the experimental results indicate a nanocrystalline iron-film embedded in a wear-resistant TiC compound. This conclusion is further supported by transmission electron microscopy studies on epitaxial Ti-Fe-C films deposited on single-crystalline MgO substrates where, upon annealing, an iron film embedded in TiC is formed. Our results suggest that annealing of metastable Ti-Fe-C films can be used as an efficient way of creating a wear-resistant magnetic thin film material.

DOI: 10.1103/PhysRevB.81.014405 PACS number(s): 75.70.−i, 75.50.Tt

I. INTRODUCTION

Thin films of the transition-metal carbides have received much attention due to their high wear resistance, low friction, and high chemical stability.[1–3] A very interesting application for this type of material is wear-resistant, low-friction magnetic coatings. Such materials could be used in, e.g., sensors and electronics. A problem with carbide-based nanocomposites is that the magnetic elements Fe, Ni, and Co are weak carbide formers and in fact only form metastable carbides although they have a high activation energy toward decomposition into graphite and metal. Furthermore, late 3*d* transition-metal carbides are less hard and wear resistant than the early 3*d* transition-metal carbides. A possible solution to this problem could be to form a solid solution of a magnetic element in a stable transition-metal carbide such as TiC. Such solid solutions may retain most of the mechanical and tribological properties (see, e.g., Refs. 2, 4, and 5) and also be tuned with respect to magnetic properties. A problem with this approach is that the solid solubility of, e.g., Fe and Ni in TiC at equilibrium is very low (<1 at. %).[6] However, it is well known that some thin film deposition processes such as magnetron sputtering at low substrate temperature can give films with very high solid solubility. For example, Wilhelmsson *et al.* have previously demonstrated that as much as 50% of the Ti in TiC can be substituted for Fe.[7] During annealing the metastable material decomposes to TiC and metallic precipitates. It was demonstrated that this concept can be used to produce wear-resistant magnetic films but no details of the influence of, e.g., temperature on the magnetic properties have yet been published. Furthermore, Trindade and Tome *et al.* have previously reported on the synthesis of thin films within the Ti-Fe-C system but the magnetic properties of this material were not measured.[8,9]

The aim of the present study is to further investigate how the magnetic properties of a $Ti_{1-x}Fe_xC_{1-y}$ film is influenced by annealing. The films have been characterized by x-ray diffraction (XRD), x-ray photoelectron spectroscopy (XPS), and superconducting quantum interference device (SQUID) magnetometry. Selected films have also been investigated by transmission electron microscopy (TEM). The experimental work is supported by first-principles density-functional theory (DFT) calculations, yielding information on exchange parameters and magnetic ordering temperatures.

II. EXPERIMENTAL

Thin films of $Ti_{1-x}Fe_xC_{1-y}$ with nominal composition $x=0.4$ and $y=0.5$ were deposited by nonreactive dc magnetron sputtering in an Ar discharge of 3 mTorr (base pressure of $<10^{-9}$ Torr). The anticipated composition was achieved by individual control of the magnetron current of the three 2″-elemental targets of Ti, Fe, and C; the purity of each target was 99.995%, 99.99%, and 99.995%, respectively. The substrate holder was held at a floating potential of about −1 V and was rotating during film growth. The films were ≈50 nm thick and deposited on amorphous quartz. Prior to deposition the substrates were ultrasonically degreased in acetone and isopropanol for 5 min each. Thereafter, they were preheated in the deposition chamber for 30 min at 450 °C followed by film growth at the same temperature. The films were postheat treated in a high-vacuum furnace (10^{-7} Torr) at 650 °C for annealing times of 2, 5, 8, 10, and 20 min.

The epitaxial $(Ti_{1-x}Fe_x)C_{1-y}$ films with nominal composition $x=0.3$ and $y=0.7$ were fabricated by the same process and postheat treated at 850 °C for an annealing time of 60 min. These films were ≈50 nm thick and deposited on single-crystalline MgO(100) substrates.

The chemical composition and elemental-chemical state of the deposited films were analyzed by XPS employing a PHI Quantum 2000 with monochromatized Al $K\alpha$ radiation. Compositional depth profiles were acquired by sequential sputtering using 4 keV Ar^+ rastered over 2×2 mm^2 area (analysis area 150 μm in diameter). Chemical composition was calculated using standard sensitivity factors provided by the instrument manufacturer. The crystal structure and crystallinity were studied by XRD using a Philips X'pert equipment (radiation Cu $K\alpha$) with a mirror on the primary side and a parallel collimator 0.27° on the secondary side. The films deposited on amorphous quartz were analyzed by grazing-incident (GI) instrumental scan geometry employing an incident angle of 0.5°.

The epitaxial films were also examined in a TEM equipped with an energy-filter system, which was used to record inelastically scattered electrons resulting in energy-filtered images (EF-TEM). For this purpose a Gatan image filter, GIF2002, was used containing a magnetic prism that bends the electrons 90° off the initial optical axis. Electrons losing different amount of energy are separated into an energy-dispersive spectrum. For elemental mapping an energy selecting slit was used for picking out a certain energy range.

Magnetization measurements were performed in a Quantum Design MPMS-XL SQUID magnetometer. Magnetization (M) versus temperature (T) was studied between 5 and 400 K following a field-cooled (FC) protocol. A weak magnetic field ($H=50$ Oe) was applied at 400 K and the magnetization was measured as the sample cooled down to 5 K. Magnetization versus field measurements were performed at 10 K between 10^4 and -10^4 Oe.

III. THEORY

First-principles DFT (Refs. 10 and 11) using the Green's-function Kohn-Korringa-Rostoker method while employing the atomic sphere approximation (ASA),[12,13] have been used in order to calculate total energies, magnetic moments, exchange parameters, and electronic structure of a number of ternary $Ti_{1-x}Fe_xC_{1-y}$ phases with varying composition of Ti, Fe, and C. The local spin-density approximation[14] was used for the exchange-correlation functional in all calculations. In case of magnetic phases, we considered only ferromagnetic ordering, even though for phase stability under annealing conditions might require more complex noncollinear magnetic configurations. This is an approximation which we expect is rather good for the present system, bearing in mind that the observed ordering temperatures are lower than deposition and annealing temperatures.

Binary TiC crystallizes in the B1 (or NaCl) structure which consists of two intersecting face-centered cubic lattices (one for Ti and one for C) shifted halfway along the body diagonal relative to each other. In order to properly fulfill the requirements for the ASA, we have introduced two empty spheres along the body diagonal of the structure.[15] Earlier studies have shown that other metals in TiC substitutes for Ti and results in a two-component metal lattice. If the other metal is a poor carbide former, such as Fe, this substitution in turn reduces the otherwise strong covalent bond between Ti and C atoms, yielding a ternary system with a lower C content than normal TiC. It is therefore necessary to calculate the magnetic properties for varying carbon content since a large number of C vacancies are present on the C lattice. The properties of substoichiometric TiC have been investigated and reported previously in Refs. 15–18.

The substitutional disorder of Fe atoms and C vacancies were treated within the coherent-potential approximation (CPA). The CPA is a single-site approximation and local environment effects are therefore neglected. These effects may have a large contribution due to local interactions and relaxations.[19] However, even though the CPA neglects local effects, the favorable properties when it comes to computational effort compared to supercell methods makes it very efficient.

The magnetic properties have been evaluated by first calculating the Heisenberg exchange parameters J_{ij} between a pair of magnetic atoms positioned at $\mathbf{R}_i$ and $\mathbf{R}_j$ according to the theory by Liechtenstein *et al.*[20] employing the magnetic force theorem, where the exchange parameters are given by

$$J_{ij} = \frac{1}{4\pi}\int^{E_F} dE\ \mathrm{Im}\{\mathrm{Tr}_L(\Delta_i T_\uparrow^{ij}\Delta_j T_\downarrow^{ij})\}, \tag{1}$$

where $\Delta_i = t_{i\uparrow}^{-1} - t_{i\downarrow}^{-1}$, t being the on-site scattering matrix and T the scattering matrix operator related to the off-diagonal elements of the Green's function. The trace in the above equation has been performed over the orbital indices of the scattering matrices. A positive (negative) J_{ij} represents a ferromagnetic (antiferromagnetic) interaction.

The Curie temperature has been calculated using both the mean-field approximation (MFA) and Monte Carlo (MC) calculations. The MFA Curie temperature is evaluated according to

$$T_c^{\mathrm{MFA}} = \frac{2x}{3k_B}\sum_{j\neq 0} J_{0j}, \tag{2}$$

where x is the concentration of magnetic atoms and k_B is Boltzmann's constant. Generally, the MFA is known to overestimate critical temperatures, especially for low concentrations of magnetic atoms.

The MC calculations have been performed using the classical zero-field Heisenberg Hamiltonian

$$H = -\sum_{i\neq j} J_{ij}\mathbf{e}_i\cdot\mathbf{e}_j, \tag{3}$$

where the magnetic exchange parameters are given by Eq. (1) and $\mathbf{e}_i$ is the unit vector of the magnetic moment at position $\mathbf{R}_i$. The simulations were performed using the single spin-flip Metropolis algorithm for varying sizes of the simulation cell and the critical temperature was obtained from the crossing of the fourth-order cumulant of the magnetization for different sizes of the simulation cell.[21]

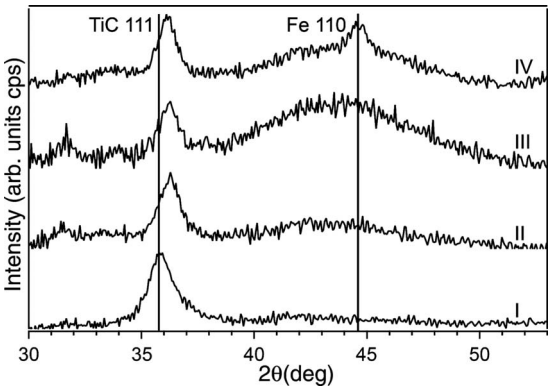

FIG. 1. X-ray diffractograms of grazing-incidence scans for the as-deposited film and films heat treated at 650 °C. I, II, III, and IV label the annealing times of 0, 5, 10, and 20 min, respectively. After 20 min of heat treatment a peak attributed to α-Fe is seen.

IV. RESULTS

A. Phase and microstructure characterization

Figures 1 and 2 show GI x-ray diffractograms and C 1*s* XPS spectra, respectively, for as-deposited and annealed films with the total composition $Ti_{0.6}Fe_{0.4}C_{0.5}$. In an earlier study such as-deposited films have been characterized in detail as a function of composition.[7] An important result was that Fe was dissolved into the carbide structure by a substitutional solid solution with Fe on the Ti sites. Furthermore, it was found that sputtered $Ti_{1-x}Fe_xC_{1-y}$ films with $y \geq 0.5$ consist of nanocrystalline (Ti,Fe)C while higher carbon contents yield a nanocomposite with nanocrystalline (Ti,Fe)C embedded in an amorphous carbon matrix. The results in Figs. 1 and 2 confirm these earlier results. The diffractogram I in Fig. 1 exhibits a (111) peak from the TiC phase with a NaCl structure. The absence of other peaks from this phase suggests a significant (111) texture. The position of the (111) peak corresponds to a unit cell that is smaller than for pure TiC (a=4.32 Å) and can be explained by a solid solution of Fe atoms into the carbide. From the Scherrer formula[22,23] the size of the (Ti,Fe)C grains can be estimated to ≈100 Å. The

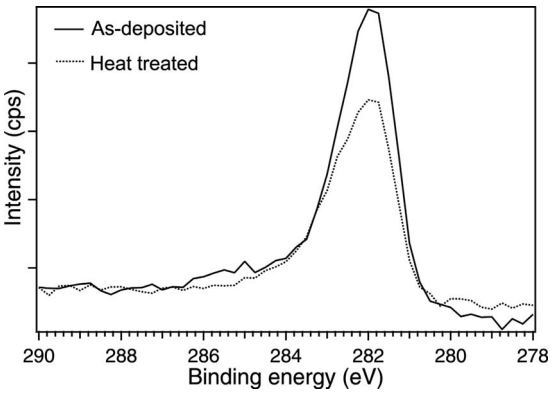

FIG. 2. C 1*s* spectrum after a short Ar^+-sputter cleaning of the surface for the as-prepared film (solid line) and for a film annealed for 20 min at 650 °C (dashed line). All heat treated films give the same result.

C 1*s* XPS spectra in Fig. 2 show only one strong peak at ≈281 eV. This peak can be attributed to Me-C bonds.[24] No indication of any significant amount of C-C bonds can be observed at 285 eV. Consequently, in agreement with the results in Ref. 7, the as-deposited films can be described as nanocrystalline films with (Ti,Fe)C nanocrystals but without any free carbon matrix.

A solid solution of $Ti_{0.6}Fe_{0.4}C_{0.5}$ is not thermodynamically stable. Titanium carbide is known to exhibit a broad homogeneity range with carbon contents in the range from $TiC_{\approx 0.97}$ to $TiC_{0.5}$. However, the maximum solid solubility of Fe is less than 1 at. %.[6] Annealing of the as-deposited $Ti_{1-x}Fe_xC_{1-y}$ film can therefore lead to two things: Initially small amounts of carbon can diffuse to the interface of the grains. The driving force for this is the rather weak Fe-C bonds in the carbide structure. The total energy of the system can be reduced by diffusion of carbon from the interior of the bulk to the surface under the formation of fairly strong C-C bonds. This effect has been experimentally demonstrated in Refs. 7 and 25 and theoretically in a paper by Råsander *et al.*[26] In the present study the $Ti_{0.6}Fe_{0.4}C_{0.5}$ films have a very low carbon content close to the limits of the homogeneity range for the pure carbide. Thus, the carbon diffusion effect should be rather small. This was also confirmed by the C 1*s* spectra in Fig. 2, showing no indication of C-C bonds after heat treatment. The second more important effect of annealing is that Fe should diffuse out from the grains and form metallic Fe precipitates. The formation of metallic Fe requires substitutional diffusion. This type of diffusion is known to have much higher activation energy, and hence a lower diffusion coefficient, than interstitial diffusion due to the need for vacancy formation. Consequently, we should expect that a $Ti_{1-x}Fe_xC_{1-y}$ film initially should exhibit some incubation time prior to the formation of metallic Fe. As can be seen in Fig. 1, clear XRD peaks from α-Fe is observed after 20 min. Moreover, as can be seen in Fig. 1 there is a gradual increase in the background intensity around $2\theta \approx 40° - 45°$ during annealing. This can be attributed to the gradual precipitation of nanocrystalline α-Fe. The exact details in phase formation from the nanocrystalline (Ti,Fe)C film to a mixture of Ti-rich carbide and Fe is not known but as will be shown below this process may be very complex.

Figure 3 shows XPS depth profiles of the $Ti_{1-x}Fe_xC_{1-y}$ films deposited on amorphous quartz. As can be seen, the atomic concentration of Ti, Fe, and C in the as-deposited state is homogeneous, while the heat treatment induces a continuous change in the elemental distribution. It can be observed that with increasing heat treatment time there is a depletion of Fe close to the surface of the film while enriched Fe regions are simultaneously formed deeper into the film. As can be seen in Fig. 3, heat treatments for 5 and 10 min, respectively, result in single regions enriched in Fe where the enriched region has moved deeper into the film after 10 min. For even longer heat treatment times two Fe-rich regions starts to develop. After 20 min of annealing two clear and well-defined regions of Fe is observed in the XPS depth profile (cf. Fig. 3). A slightly increased surface oxidation is also noted for the annealed samples. XPS results indicate that the oxygen is predominantly bonded to Ti. From the XRD analysis it is also evident that the observed redistribu-

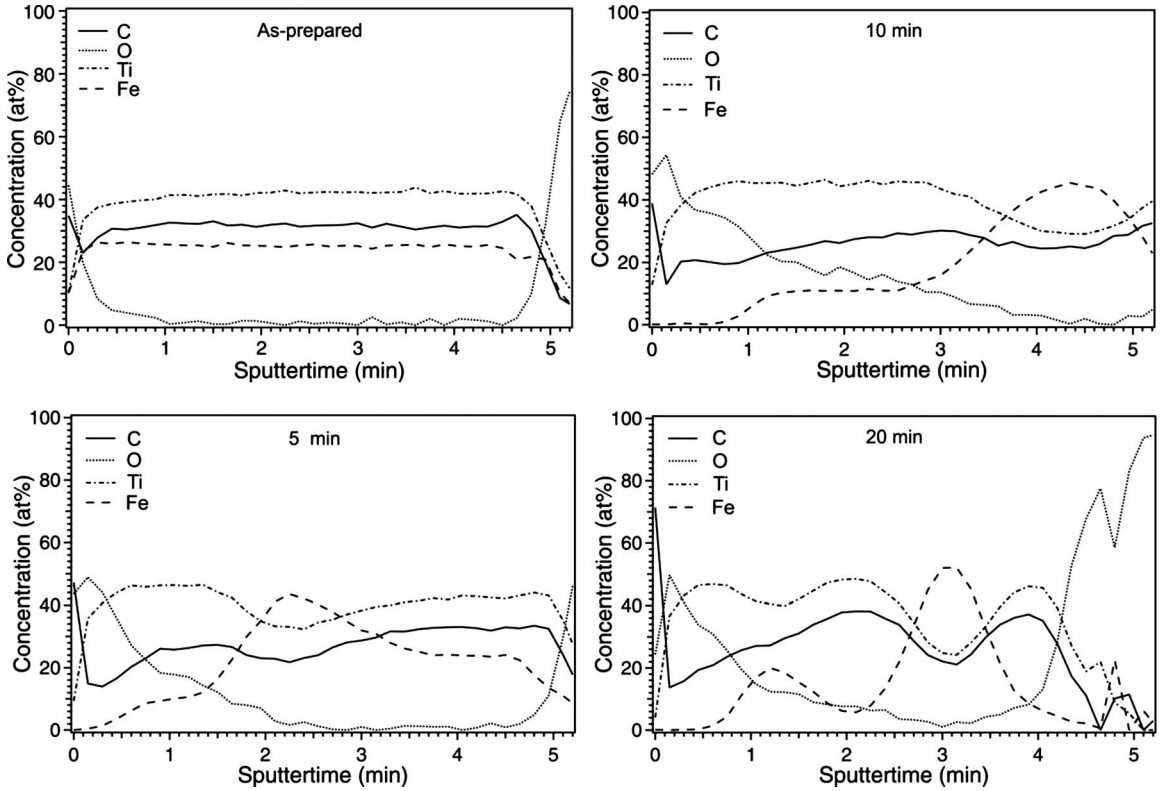

FIG. 3. XPS depth profiles vs Ar^+ sputtering time for the as-deposited film and for films after 5, 10, and 20 min annealing at 650 °C. Annealing results in composition inhomogeneity and regions with different Fe content.

tion and enrichment of Fe improves the crystallinity of the precipitating α-Fe phase. As a matter of fact a clear Fe(110) diffraction peak is observed after 20 min of heat treatment (see Fig. 1).

The XRD and XPS results presented above agree very well with TEM results obtained from studies on $Ti_{1-x}Fe_xC_{1-y}$ films deposited on single-crystalline MgO(100) substrates.[27] These films have been grown epitaxially on the MgO(100) substrate and forms, in similarity with the results obtained for amorphous quartz substrates in the present study, regions of α-Fe upon vacuum-heat treatment. An illustrative example can be seen in Fig. 4 where cross-sectional energy-filtered TEM images of Ti, Fe, and C are shown. The EF-TEM images clearly show that by annealing, the near surface region as well as the region close to the substrate is depleted in Fe and more similar to pure TiC and that an $\approx$10 nm thick Fe rich layer is formed in between. Moreover, XRD results[27] as well as results from field-dependent magnetization measurements [cf. Fig. 7(b)] indicate that the Fe layer is predominantly made up of α-Fe.

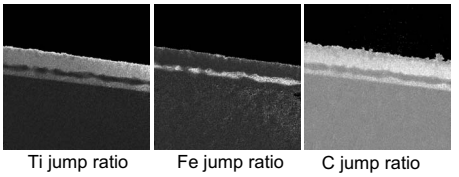

FIG. 4. EF-TEM images of a (Ti,Fe)C film deposited on a single-crystalline MgO(100) substrate and heat treated for 60 min at 850 °C, showing regions with high concentrations of α-Fe, Ti, and C. Brighter contrast indicates higher element concentration.

B. Magnetic characterization

Figure 5 shows the temperature dependence of the magnetization in the temperature range from 5 to 400 K for the as-deposited film and for the different annealing times ranging from 2 to 10 min. The as-deposited film exhibits a clear sign of magnetic ordering with an ordering temperature of $\approx$50 K. As can be seen in the figure the magnetic behavior is strongly dependent on heat treatment time. Even for as small annealing time as 2 min, the low-field magnetization is much larger in magnitude and more importantly there is a strong increase in the magnetic ordering temperature up to

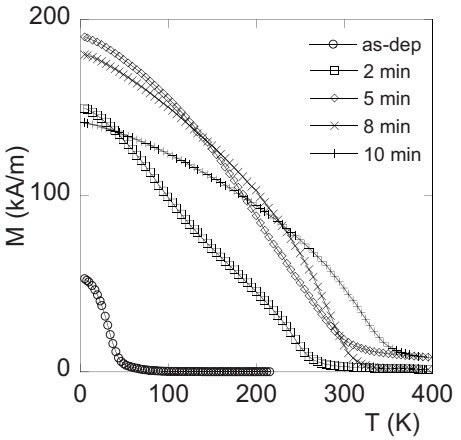

FIG. 5. Temperature dependence of the FC magnetization with an applied field of 50 Oe for different annealing times at 650 °C. T_c increases with annealing time.

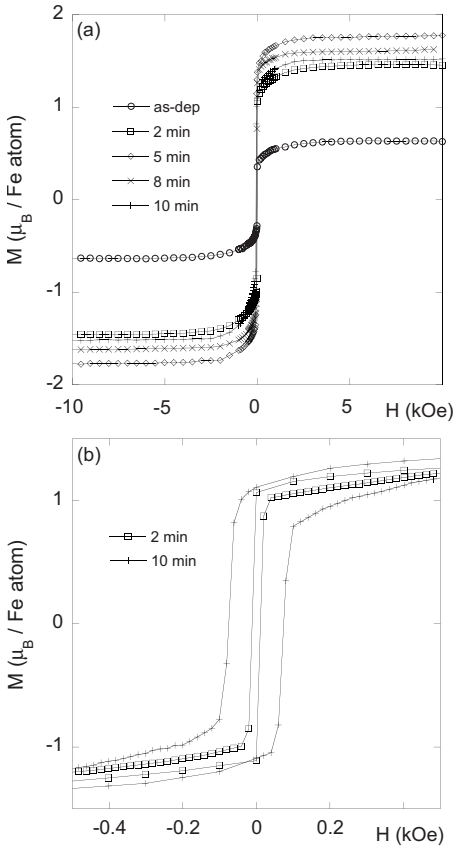

FIG. 6. (a) Field dependence of the magnetization for different annealing times at 650 °C. (b) The coercivity increases due to formation of α-Fe nanocrystals.

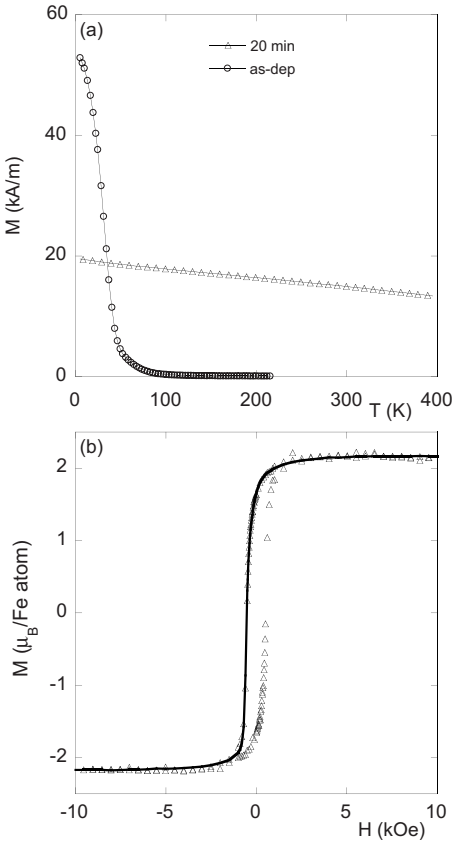

FIG. 7. (a) Magnetization vs temperature for the as-deposited film and the film annealed for 20 min at 650 °C. T_c for the annealed film is far above 400 K. (b) The coercivity for the annealed film increases significantly due to formation of α-Fe nanocrystals (open triangles). Magnetization vs field for the epitaxial film deposited on a single-crystalline MgO substrate and annealed at 850 °C for 60 min is included for comparison (thick solid line), showing the magnetization values sweeping the field from +10 to −10 kOe.

≈250 K. Moreover, the heterogeneous composition of the annealed film, as seen in the previously discussed XPS results, is reflected in the two-steplike magnetic transition, a feature which is also observed for 5 min of annealing. For 10 min of heat treatment, the magnetic ordering temperature has reached ≈350 K, and there is no clear sign of a two-steplike magnetic transition in the experimental temperature window. However, the low-field magnetization remains comparably large in magnitude above the magnetic ordering temperature, which gives further support for the precipitation of nanocrystalline α-Fe after sufficiently long annealing time. Thus, by carefully tuning the annealing time it can be claimed that the T_c value for the $Ti_{1-x}Fe_xC_{1-y}$ substitutional solid solution can be increased up to approximately 350 K.

Figure 6(a) shows a comparison of the field dependence of the magnetization at 10 K for the as-deposited and annealed films. After heat treatment, the saturation magnetization (M_s) has increased for all films. This is explained by the composition inhomogeneity created by the heat treatment yielding regions with increased iron (x) and C-vacancy concentrations (y). The saturation magnetization is highest for the 5 min heat treatment film and slowly decreases as nanocrystalline α-Fe starts to form. The decrease in the saturation magnetization is explained by partial formation of a weakly magnetic but not yet identified intermediate product of the decomposition of $Ti_{1-x}Fe_xC_{1-y}$ into TiC_{1-y} and α-Fe. Figure 6(b) shows that the coercivity increases from less than 20 Oe for 2 min to 100 Oe for 10 min heat treatment indicating an increase in film defect density as a result of the heterogeneous film composition.

Figure 7(a) shows that after 20 min annealing the most of the Fe content has formed α-Fe nanocrystals since there is no sign of a magnetic ordering temperature in the experimental temperature window and T_c for the α-Fe phase is much higher than the upper boundary of the temperature window. Another confirmation of the α-Fe phase is that the magnetic moment has increased to $\approx 2.1\mu_B$/Fe atom, as seen in Fig. 7(b). Moreover, the coercivity has increased to 500 Oe, which is not unexpected considering the nanocrystalline character of this phase and the shape anisotropy of the nanocrystals. For comparison, the magnetization vs field results for the annealed epitaxial film has been included in the same figure, yielding the same magnetic moment ($\approx 2.1\mu_B$/Fe atom) at magnetic saturation. This result fortifies the interpretation of the EF-TEM images shown in Fig. 4 that the Fe rich layer is predominantly made up of α-Fe. It is interesting to note that both annealed films, i.e., the films deposited on amorphous quartz (annealed for 20 min at 650 °C) and single-crystalline MgO (annealed for 60 min at 850 °C) substrates, exhibit almost identical coercive fields, which indi-

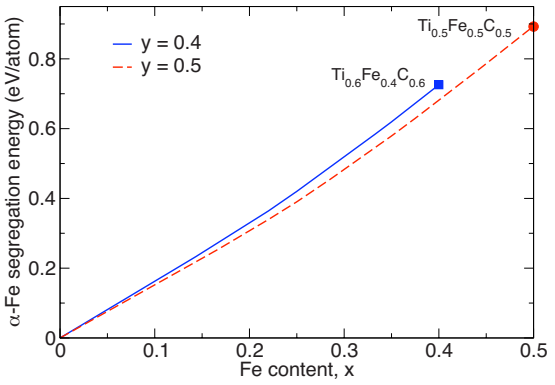

FIG. 8. (Color online) Energy gained by releasing Fe from $Ti_{1-x}Fe_xC_{1-y}$ in the form of α-Fe for $y=0.4$ and 0.5, obtained according to Eq. (4).

cates that the Fe layers have very similar properties with respect to size, shape, and packing of α-Fe nanocrystals.

C. Theoretical results

The experimental results suggest that precipitates of Fe is formed upon annealing and in order to support these findings we have analyzed the energy for α-Fe segregation from $Ti_{1-x}Fe_xC_{1-y}$ which is evaluated according to

$$E_s(\alpha\text{-Fe}) = E(Ti_{1-x}Fe_xC_{1-y}) - (1-x)E(TiC_z) - xE(\alpha\text{-Fe}), \tag{4}$$

where $z=\frac{1-y}{1-x}$. The results of Eq. (4) are given in Fig. 8 for two values of y ($y=0.4$ and $y=0.5$). It is clear that by increasing the Fe concentration it is energetically more favorable for Fe to segregate from the carbide and form α-Fe. This holds for all considered values of x and y, and demonstrates that the films considered experimentally here are all metastable. The results of Fig. 8 are consistent with the low solubility of Fe in bulk TiC.

In Fig. 9 we show the calculated magnetic moments for the Fe atoms in $Ti_{0.75}Fe_{0.25}C_{1-y}$ and $Ti_{0.65}Fe_{0.35}C_{1-y}$ along with the calculated critical temperatures from both MC and MFA. We also show calculated data points for two specific compositions, namely, $Ti_{0.52}Fe_{0.48}C_{0.37}$ and $Ti_{0.78}Fe_{0.22}C_{0.47}$, corresponding to regions of high and low Fe concentrations (cf. Fig. 3), respectively. The general trend is that the magnetic moment and ordering temperature both increase with increasing Fe content. The same is true when increasing the C vacancy concentration although the effect is much stronger when increasing the Fe content. We also note that the MFA gives larger values than MC for the ordering temperatures. It is important to note here that the data from MC are expected to be more accurate. Focusing on the curve for $Ti_{0.65}Fe_{0.35}C_{1-y}$, which is the one closest resembling our experimental sample, we see that the magnetic moment and MFA ordering temperature have a similar increasing behavior as a function of C vacancy concentration, while the MC ordering temperature stays more or less constant at about 130–135 K for low vacancy concentrations with an increase to 165 K for $y=0.5$. Furthermore, there is an initial descent

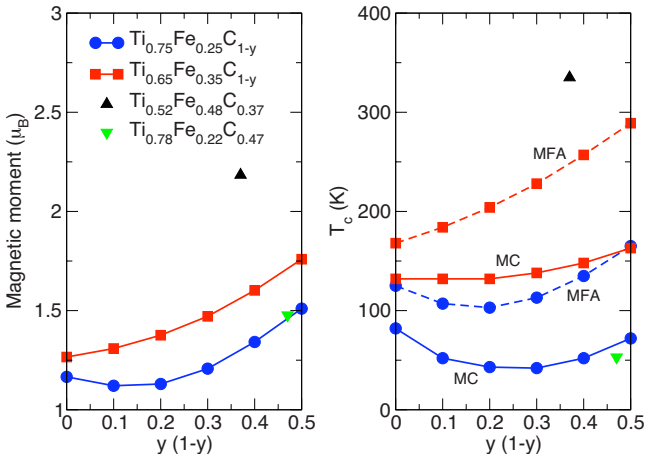

FIG. 9. (Color online) Calculated magnetic moments (left panel) and critical temperatures (right panel) from both mean field and Monte Carlo simulations as a function of carbon vacancy concentration, y, for different Fe concentrations, x. The MC data for the critical temperatures are drawn with a solid line while the corresponding MFA values are drawn with a dashed line. For the specified compositions $Ti_{0.52}Fe_{0.48}C_{0.37}$ and $Ti_{0.78}Fe_{0.22}C_{0.47}$ only MC values are given. These are in the figure plotted as a function of the carbon concentration 1-y.

in the value for the magnetic moment and ordering temperature for $x=0.25$, which will become apparent when considering the behavior of the magnetic exchange parameters. However, it is still valid to conclude that by increasing the Fe content or the C vacancy concentration the magnetic moment as well as the ordering temperature increases.

By comparing the calculated magnetic moments and ordering temperatures to the experimentally determined values we note that upon annealing between 2 and 10 min the magnetic moment of the Fe atoms varies between $1.43\mu_B$ and $1.82\mu_B$ and the ordering temperature varies from 270 to 360 K. The theoretical results obtained for $x=0.35$ and $y=0.5$ give a moment of $1.76\mu_B$ and an ordering temperature of 165 K. The calculated moment is within the experimental interval but the calculated ordering temperature is somewhat too low. However, since the annealed samples show regions of different compositions, as shown by the XPS depth profiles, this has to be taken into consideration. The theoretically considered compositions of high ($x=0.48$, $y=0.63$) and low ($x=0.22$, $y=0.53$) Fe concentrations correspond to regions found in the sample after 5 min of annealing. Here the experimentally obtained ordering temperature is 310 K. The calculated ordering temperatures are 340 and 50 K for the Fe-rich and Fe-poor compositions, respectively. It has been shown[28] that for magnetic composites the ordering temperature is close to the highest value of the materials forming the composite, i.e., 340 K in our case, and bearing this in mind one can conclude that there is good agreement between the experimentally obtained ordering temperature and the theoretical value.

The experimentally obtained magnetic moment is $1.82\mu_B$ while the theoretical moments are $2.18\mu_B$ (Fe rich) and $1.48\mu_B$ (Fe poor). Considering that the experimentally obtained moment is an averaged quantity (total magnetization

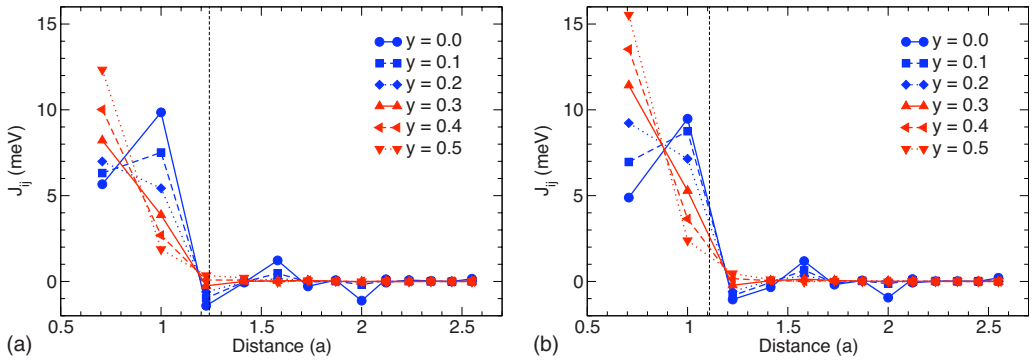

FIG. 10. (Color online) Calculated exchange parameters for $Ti_{1-x}Fe_xC_{1-y}$ with (a) $x=0.25$ and (b) 0.35. Note the oscillating behavior for low vacancy concentration, where the strength of the nearest-neighbor interaction is lower than the second neighbor interaction for $y=0$ and 0.1, while the exchange interaction is rapidly decreasing for the higher vacancy concentrations. The dotted vertical line indicates the average distance between Fe atoms for the corresponding concentrations.

divided by the number of Fe atoms per unit volume) over the whole sample, we compare this value with the average between the theoretical values for Fe-rich and Fe-poor regions, assuming equal volumes for the two regions, given by $\bar{\mu} = (\mu_{\text{Fe-rich}} + \mu_{\text{Fe-poor}})/2 = 1.83\mu_B$. This averaged moment is in good agreement with the experimentally obtained moment. According to the above discussion we conclude that the theoretically obtained magnetic moments and ordering temperatures are in good agreement with experiment when considering that the experimental sample consists of regions of both Fe-rich and Fe-poor regions.

The calculated magnetic exchange parameters, which were used in the evaluation of the ordering temperatures, are presented in Fig. 10. The most apparent fact is that the exchange parameters for low carbon vacancy concentrations ($y=0$, 0.1, and 0.2) oscillate between positive and negative values, meaning that the interaction is ferromagnetic or antiferromagnetic depending on the distance between magnetic atoms. For even greater C vacancy concentrations the interaction is rapidly decreasing with increasing distance between magnetic atoms. Furthermore, the nearest-neighbor interaction is lower than the second-nearest-neighbor interaction for low C-vacancy concentration, while there is a change in behavior for $y \geq 0.2$, where the nearest-neighbor interaction is stronger. This is reasonable considering the B1 crystal structure and the chemical bonding of TiC. The nearest-neighbor Fe-Fe interaction distance is given by $a/\sqrt{2}$, where a is the lattice parameter of the primitive cell, while the second nearest neighbor is at a distance a away. If the system would have been a binary TiFe alloy on a regular face-centered cubic lattice there would have been a considerable d-orbital overlap between nearest-neighbor metal atoms. However, this is not the case in ternary $Ti_{1-x}Fe_xC_{1-y}$, since the inclusion of a carbon lattice has increased the volume of the system resulting in a reduced d-band overlap between the atoms on the metal lattice.[29] The chemical bonding in TiC is primarily due to strong covalent bonds formed by Ti d and C p electrons separated by a distance $a/2$ from each other. The second-nearest-neighbor interaction for a Fe atom in $Ti_{1-x}Fe_xC_{1-y}$ is along the direction of the covalent bond, yielding a stronger magnetic interaction due to the significant orbital overlap along this direction. However, if there is a substantial number of C vacancies the covalent bonding between metal atoms and carbon will give way for a larger d-band overlap between neighboring metal atoms, therefore changing the relative strength of the magnetic interaction between first- and second-shell neighbors, which can readily be observed in Fig. 10.

Furthermore, by comparing the exchange parameters for $x=0.25$ and $x=0.35$ we conclude that the exchange parameters are generally stronger for $x=0.35$ which is shown most prominently in the first neighbor interaction in Fig. 10, especially for high vacancy concentrations. This is the reason for the higher ordering temperatures shown in Fig. 9 for the phases with a higher Fe concentration. Figure 10 also shows that the average distance between Fe atoms in the system lies in regions of different behavior of the exchange parameters. For $x=0.25$ the average distance lies in a region of antiferromagnetic coupling between Fe atoms for $y \leq 0.2$ and a very low ferromagnetic coupling for $y \geq 0.2$. When the Fe concentration is increased to $x=0.35$ the averaged distance between Fe atoms are in a position of ferromagnetic coupling for all y within the calculated range. It is therefore possible to conclude that the ferromagnetic properties of $x=0.35$ is greater than for $x=0.25$ which is readily seen in Fig. 9. From the exchange parameters for $x=0.25$ we also note that the next-nearest-neighbor interaction goes down faster than the increase in the nearest-neighbor interaction for $y \leq 0.2$. This is the reason for the initial descent of the ordering temperature for $x=0.25$.

In Fig. 11 we show the calculated density of states (DOS) for each atom type in $Ti_{0.65}Fe_{0.35}C_{1-y}$, for two different vacancy concentrations ($y=0$ and 0.5). When there are no C vacancies present there are two distinct peaks in the DOS for Fe, both in the majority and minority spin channels. By increasing the number of C vacancies these peaks move closer together and furthermore the middle of each Fe band has moved to lower (majority-spin) and higher (minority-spin) energies. This increased shift in the band centers for majority and minority spin channels is responsible for the increased magnetic moment when decreasing the amount of C in the system. At the same time the Ti DOS has become broader and moved toward lower energies for both spin channels. This signifies a more pronounced d-orbital overlap between

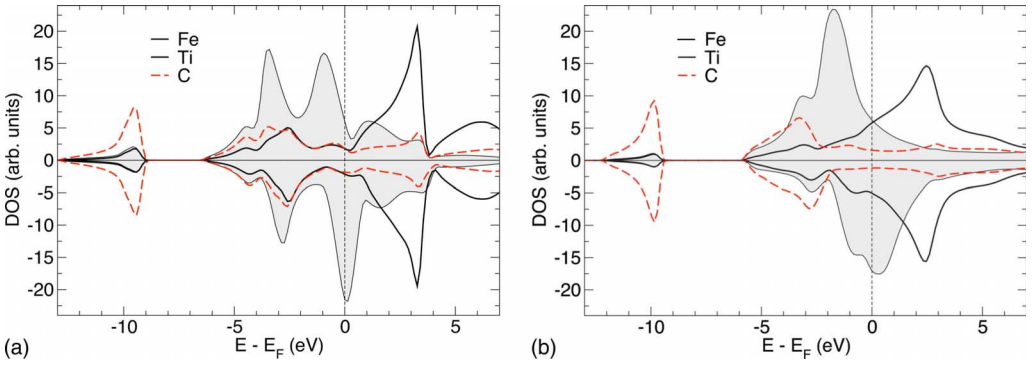

FIG. 11. (Color online) Projected DOS for $Ti_{0.65}Fe_{0.35}C_{1-y}$ for (a) $y=0$ and (b) 0.5. The Fermi level is indicated by a solid vertical line and the scale on the y axis is the same for each of the DOS. The DOS for Fe are filled with gray color for clarity.

Ti atoms for higher C-vacancy concentrations, consistent with the previous discussion for the exchange parameters. The DOS at about −10 eV which is dominated by C 2*s* states has become narrower and with a lower DOS for Ti and Fe states in this region which further supports the argument of less pronounced bonding between metal atoms and C.

V. SUMMARY AND CONCLUSIONS

Thin films of $Ti_{1-x}Fe_xC_{1-y}$ have been demonstrated to be obtained by magnetron sputtering. In these films, a solid substitutional solution is formed where Fe replaces Ti in the TiC structure. The films can be deposited in a wide range of compositions with respect to both carbon and metal content. At high Fe contents, metallic α-Fe forms precipitations. α-Fe formation as nanocrystallites is also favored by a long deposition time and by a postannealing at 650–850 °C. TEM studies on epitaxial samples on single-crystalline MgO substrates (Fig. 4) suggest that, by annealing, the near surface region as well as the region close to the substrate is depleted in Fe and more similar to pure TiC.

The results are further supported by XPS studies (Fig. 3) where it can be seen how the element composition changes as a result of heat treatment. All elements seemingly redistribute during heat treatment and with enough annealing an α-Fe layer, embedded in TiC depleted in Fe, is formed close to the substrate surface (cf. Figs. 3 and 4). These experimental findings are in agreement with our first-principles theory calculations, which show that Fe doped in a TiC film becomes a metastable system. The experimental results indicate that the formation of α-Fe is blocked during the early stages of annealing but that the formation of nanocrystalline α-Fe will prevail after long enough annealing time.

The magnetic properties of the Fe-doped TiC films have also been investigated experimentally and theoretically. We show that the magnetic moment and ordering temperature are rather substantial, at least for the concentrations of Fe considered here. The interatomic exchange interactions have also been analyzed and found to reflect the underlying chemical bonding of the material. The trend of α-Fe to form as a separate layer inside the TiC matrix, is an interesting avenue to grow magnetic trilayers or multilayers by a repetition of the growth procedure presented here and subsequent heat treatment. The results of such a study are outside of the scope of the present paper.

ACKNOWLEDGMENTS

We acknowledge support from the Swedish Research Council, Swedish Foundation for Strategic Research, and the Swedish National Allocations Committee.

[1] R. Hauert and J. Patscheider, Adv. Eng. Mater. **2**, 247 (2000).
[2] *Nanostructured Coatings*, edited by A. Cavalerio and J. T. M. DeHosson (Springer Science+Buisness Media LLC, New York, 2006).
[3] D. Martínez-Martínez, C. López-Cartes, A. Fernández, and J. C. Sánchez-López, Thin Solid Films **517**, 1662 (2009).
[4] K. Hono, N. Hasegawa, S. S. Babu, H. Fujimori, and T. Sakurai, Appl. Surf. Sci. **67**, 391 (1993).
[5] N. Hasegawa, A. Makino, N. Kataoka, H. Fujimori, A. P. Tsai, A. Inoue, and T. Masumoto, Mater. Trans., JIM **36**, 952 (1995).
[6] P. Vilars, A. Prince, and H. Okamoto, *Handbook of Ternary Alloy Phase Diagrams* (ASM International, London, 1995), Vol. 5.
[7] O. Wilhelmsson, S. Bijelovic, M. Lindquist, B. Andre, U. Wiklund, P. Svedlindh, and U. Jansson, Thin Solid Films (to be published).
[8] G. Tomé, B. Trindade, and M. T. Vieira, Vacuum **64**, 205 (2002).
[9] B. Trindade and M. T. Vieira, Mater. Sci. Eng., A **352**, 195 (2003).
[10] H. Hohenberg and W. Kohn, Phys. Rev. **136**, B864 (1964).
[11] W. Kohn and L. J. Sham, Phys. Rev. **140**, A1133 (1965).
[12] I. A. Abrikosov and H. L. Skriver, Phys. Rev. B **47**, 16532 (1993).
[13] A. V. Ruban and H. L. Skriver, Comput. Mater. Sci. **15**, 119 (1999).
[14] J. P. Perdew, K. Burke, and M. Ernzerhof, Phys. Rev. Lett. **77**, 3865 (1996).
[15] P. A. Korzhavyi, L. V. Pourovskii, H. W. Hugosson, A. V. Ruban,

and B. Johansson, Phys. Rev. Lett. **88**, 015505 (2001).
[16] H. W. Hugosson, P. A. Korzhavyi, U. Jansson, B. Johansson, and O. Eriksson, Phys. Rev. B **63**, 165116 (2001).
[17] K. E. Tan, A. M. Bratkovsky, R. M. Harris, A. P. Horsfield, D. Nguyen-Manh, D. G. Pettifor, and A. P. Sutton, Modell. Simul. Mater. Sci. Eng. **5**, 187 (1997).
[18] L. E. Toth, *Transition Metal Carbides and Nitrides* (Academic, New York, 1971).
[19] B. Alling, A. V. Ruban, A. Karimi, O. E. Peil, S. I. Simak, L. Hultman, and I. A. Abrikosov, Phys. Rev. B **75**, 045123 (2007).
[20] A. I. Liechtenstein, M. I. Katsnelson, V. P. Antropov, and V. A. Gubanov, J. Magn. Magn. Mater. **67**, 65 (1987).
[21] D. P. Landau and K. Binder, *A Guide to Monte Carlo Simulations in Statistical Physics* (Cambridge University Press, Cambridge, 2000).
[22] B. D. Cullity, *Elements of X-Ray Diffraction*, 2nd ed. (Addison-Wesley, Reading, MA, 1978).
[23] P. Scardi, M. Leoni, and R. Delhez, J. Appl. Crystallogr. **37**, 381 (2004).
[24] *Handbook of X-Ray Photoelectron Spectroscopy*, edited by J. Chastain and R. C. J. King (Physical Electronics, Eden Prairie, 1995).
[25] O. Wilhelmsson, M. Råsander, M. Carlsson, E. Lewin, B. Sanyal, U. Wiklund, O. Eriksson, and U. Jansson, Adv. Funct. Mater. **17**, 1611 (2007).
[26] M. Råsander, M. Klintenberg, B. Sanyal, E. Lewin, O. Wilhelmsson, U. Jansson, and O. Eriksson (unpublished).
[27] O. Wilhelmsson, S. Bijelovic, M. Lindquist, B. Andre, P. Svedlindh, and U. Jansson Thin Solid Films (to be published).
[28] R. Skomski and D. J. Sellmyer, J. Appl. Phys. **87**, 4756 (2000).
[29] C. D. Gelatt, A. R. Williams, and V. L. Moruzzi, Phys. Rev. B **27**, 2005 (1983).